Antiferromagnetic ground state and heavy-fermion behavior in Ce_2Pt_2Pb

N. Kabeya,[1,2,*] S. Takahara,[1] N. Satoh,[1] S. Nakamura,[2,3] K. Katoh,[4] and A. Ochiai[1,2]
[1]*Department of Physics, Tohoku University, Sendai 980-8578, Japan*
[2]*Center for Low Temperature Science, Tohoku University, Sendai, 980-8578, Japan*
[3]*Institute for Materials, Tohoku University, Sendai 980-8577, Japan*
[4]*Department of Applied Physics, National Defense Academy, Yokosuka 239-8686, Japan*

(Received 3 August 2017; revised manuscript received 22 June 2018; published 20 July 2018)

Specific heat, magnetization, and electrical resistivity have been studied on single crystalline samples of Ce_2Pt_2Pb. These results clearly indicate that Ce_2Pt_2Pb undergoes an antiferromagnetic transition at approximately 3.4 K under a zero magnetic field. The magnetic field induces another ordered phase when the field is applied along the ⟨100⟩ or ⟨110⟩ directions of the crystallography, whereas we have not found another ordered phase along the ⟨001⟩ direction of the field. The specific heat and the magnetization along three directions of the field reveal an easy-plane type magnetic anisotropy even in the antiferromagnetic phase. The magnetic structures of the ordered phases are discussed from the standpoint of macroscopic measurement, which results in a helical magnetic structure as a reasonable scenario. A large Sommerfeld coefficient of the specific heat and squared-temperature dependence of the electrical resistivity strongly suggest construction of the heavy-fermion state in Ce_2Pt_2Pb, while the influence of the frustration is hardly found.

DOI: 10.1103/PhysRevB.98.035131

I. INTRODUCTION

Geometrical frustration between magnetic moments has been attracting a great deal of attention because it can lead to novel ground states such as spin liquid [1]. Recent studies have discovered that the quantum fluctuation induced by the frustration possibly yields not only entirely new ground states but also key features for understanding Fermi surface reconstruction in heavy-fermion systems [2–6]. These investigations have revealed that the quantum fluctuation induced by the frustration plays a crucial role in determining the properties of ground states. Furthermore, the frustration may also become one of the key features for understanding the Fermi surface reconstruction in heavy-fermion systems.

The intermetallic Ln_2T_2X compounds, where Ln = rare earth element, T = transition metal, and X = main group metal, may offer a suitable experimental model to research the problem. Most of these compounds crystallize in the Mo_2FeB_2-type structure with the space group $P4/mbm$ (space group number 127; see insets of Fig. 1) [7,8]. In this structure, rare earth elements are located on a geometrically frustrated arrangement equivalent to the Shastry-Sutherland (SS) model that yields an antiferromagnetic order or a magnetic dimer state depending on the ratio of the exchange interactions between the nearest- and the next-nearest-neighbor moments [9]. Ln_2T_2X compounds exhibit a variety of phenomena, for instance, intermediate valence [10], antiferromagnetic and/or ferromagnetic ordering [11,12], spin glass [13], partially broken order and spinon distribution [14,15], and possible quantum criticality [16].

Among the Ln_2T_2X compounds, Ce_2Pt_2Pb is attracting attention because a nontrivial origin of quantum criticality is proposed. From an investigation using polycrystalline samples of Ce_2Pt_2Pb [16], it has been reported that (i) the magnetic susceptibility exhibits no anomaly at least above 1.8 K, (ii) the specific heat shows only a small broad peak at approximately 2 K, and (iii) the electrical resistivity is almost temperature independent below 300 K. Because the specific heat shows no singular anomaly, the authors of the paper have attributed the broad peak to the singlet-triplet excitation of the dimerized nearest-neighbor moments of the Ce^{3+} ions. The temperature-independent resistivity can possibly be attributed to localized quasiparticles by strong fluctuation. Consequently, Ce_2Pt_2Pb has been reported to be a candidate compound that is located in the vicinity of a quantum critical point (QCP) driven by the geometrical frustration.

However, intrinsic properties are sometimes disturbed by a large number of grain boundaries in the polycrystalline sample. Therefore synthesizing single crystalline samples of Ce_2Pt_2Pb has been required for further research. Furthermore, because competition between the geometrical frustration and the Kondo effect is still an open question, intriguing properties in this compound should be discussed from both standpoints. In this paper, we present a method of growing the single crystalline Ce_2Pt_2Pb and report its powder x-ray diffraction (XRD), specific heat, magnetization, electrical resistivity, and H-T phase diagrams. Our finding clearly indicates an antiferromagnetic long-range order and heavy-fermion behavior in Ce_2Pt_2Pb.

II. SAMPLE PREPARATION AND EXPERIMENTAL METHOD

Single crystalline samples of Ce_2Pt_2Pb were successfully grown by the Bridgman method from stoichiometric starting

*kabeya.noriyuki@mail.clts.tohoku.ac.jp

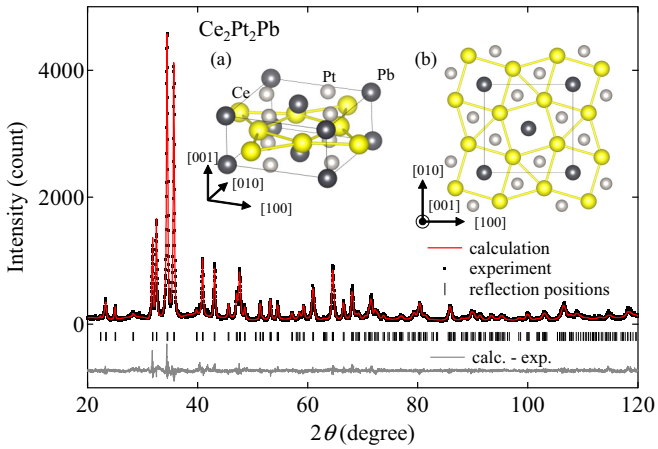

FIG. 1. X-ray diffraction pattern of Ce_2Pt_2Pb and its Rietveld analysis. Inset figures (a) and (b) show the crystal structure of Ce_2Pt_2Pb. (a) Diagonal view of atoms in a unit cell with four Ce atoms in nearest neighbor unit cells. A rectangular cuboid with solid lines represents the unit cell. (b) Planar view from the ⟨001⟩ direction. The solid lined square represents the unit cell.

materials (3N Ce, 3N5 Pt, and 5N Pb) by employing the following procedure. First, several pieces of the starting materials were sealed in a tungsten crucible using an electron-beam welder under high vacuum. Then, the sealed crucible was heated up to 1600 °C in a tungsten-mesh heater furnace. Finally, the crucible was slowly (2 mm/hour) removed from the heater. The powder XRD pattern was obtained using a Bragg-Brentano diffractometer with the CuK_α radiation. Rietveld analysis of the diffraction pattern was performed by the RIETAN-FP program. Single crystalline samples cut from the ingot were shaped using a polisher after being oriented by x-ray Laue backscattering. Single crystalline samples of La_2Pt_2Pb were also obtained by a similar method as the one described above. Magnetization measurements were performed using a superconducting quantum interference device magnetometer (MPMS, Quantum Design) between 1.8 K and 300 K. Specific heat measurements were performed by using two different methods, the dual-slope method (PPMS, Quantum Design) and the quasiadiabatic method (handmade calorimeter). The dual-slope method was used for temperatures from 2 K to 300 K with zero magnetic field, while the quasiadiabatic method was used between 0.2 K and 5 K with fields up to 15 T. The electrical resistivity was measured using the conventional four-wired method.

III. EXPERIMENTAL RESULTS

A. Powder x-ray analysis

The x-ray powder diffraction pattern and its Reitveld refinement are shown in Fig. 1. From the refinement, it is confirmed that the resultant ingot has the Mo_2FeB_2 structure with the lattice constants $a = 7.9466(18)$ Å and $c = 3.8104(9)$ Å. The lattice constant c is slightly smaller than the reported value [7]. The obtained structural parameters are listed in Table I. Reliability indices and a goodness-of-fit indicator are obtained as $R_{wp} = 9.99$, $R_e = 7.45$, $R_B = 2.82$, $R_F = 1.51$, and $S = 1.34$, where the indices R_{wp}, R_e, R_B, R_F, and S are the agreement factor concerning weighed profile intensities, the expected value from counting statistic, the R-Bragg factor, the R-structure factor, and the goodness of fit, respectively. From our analysis, neither atomic replacements nor imperfectly filling sites that exceed two standard deviations are found.

TABLE I. Refined atomic positions and the isotropic displacement parameter U_{iso} for Ce_2Pt_2Pb.

Atom	Wyckoff site	x	y	z	U_{iso} (pm^2)
Ce	4h	0.1755(2)	$x + 1/2$	1/2	47(5)
Pt	4g	0.3753(2)	$x + 1/2$	0	100(4)
Pb	2a	0	0	0	105(5)

B. Magnetic susceptibility

Figure 2 shows the temperature dependences of the magnetization divided by the magnetic field M/H (susceptibility). The field is applied in three symmetrical directions, along ⟨100⟩, ⟨110⟩, and ⟨001⟩ in the tetragonal crystal. The susceptibility along these three directions increases with decreasing temperature below 300 K after which it exhibits an obvious kink at $T_N = 3.5$ K. This feature implies that the ground state of Ce_2Pt_2Pb corresponds to an antiferromagnetic order. Below T_N, the susceptibility along the ⟨100⟩ and ⟨110⟩ directions decreases with decreasing temperature, while that along the ⟨001⟩ direction retains almost the same value. These temperature dependences imply that the magnetic moments lie within the (001) plane in the ordered state. A similar susceptibility is also reported in Ce_2Ge_2Mg below 100 K [16].

Below approximately 70 K, the susceptibility along the ⟨100⟩ and ⟨110⟩ directions is larger than that along the ⟨001⟩ direction as shown in the main panel. Above the temperature,

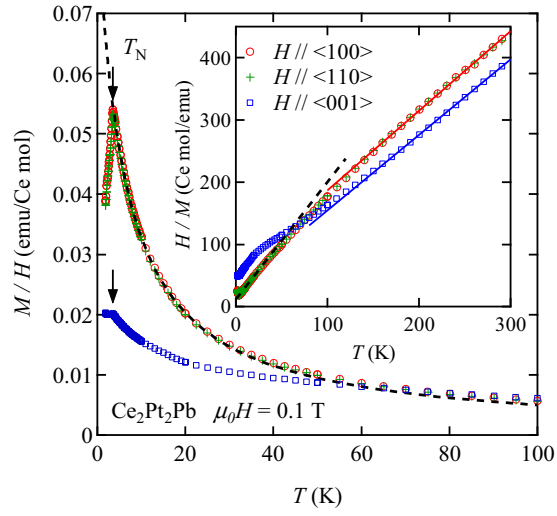

FIG. 2. Temperature dependences of magnetization divided by the magnetic field M/H along the ⟨100⟩, ⟨110⟩, and ⟨001⟩ directions. The arrows represent a phase transition temperature T_N. Inset shows the reciprocal susceptibility H/M. The solid and dotted lines are the Curie-Weiss (CW) fitted curves. The CW curves are fitted for the data along the ⟨110⟩ and ⟨001⟩ directions. A common legend is used for the main and the inset panels.

the relationship between their magnitudes is interchanged as shown in the inset of Fig. 2. The anisotropic susceptibility and its temperature dependence strongly indicate the influence of the crystal electric field (CEF). In Ce_2Pt_2Pb, the cerium site has the point group symmetry C_{2v}. The CEF belonging to C_{2v} splits the energy of the sixfold degenerate $J = 5/2$ multiplet of the Ce^{3+} ions to three doublets that have different anisotropic magnetic moments. The results of anisotropic susceptibility in Ce_2Pt_2Pb mean that the ground state of the J multiplet has a large magnetic moment along the (001) plane. No significant difference is found between the ⟨100⟩ and ⟨110⟩ directions of the susceptibility because of the tetragonal symmetry of Ce_2Pt_2Pb. As a result, our analysis using the susceptibility and specific heat cannot determine the wave functions under the CEF.

The reciprocal susceptibility also provides us information about the effective magnetic moment and the Weiss temperature. The solid and broken lines in the inset of Fig. 2 represent the results of the curve fittings to the Curie-Weiss (CW) law within the temperature ranges 4 K to 20 K and 150 K to 300 K, respectively. Note that we neglected a temperature-independent susceptibility for the curve fittings; that is, the formula $H/M = (T - \theta_P)/C$ is used for the fitting function, where θ_P and C are the Weiss temperature and the Curie constant, respectively. The effective magnetic moment μ_{eff} is obtained from the curve fitting between 150 K and 300 K, where the susceptibility includes the contribution of the excited CEF states. We obtain μ_{eff} as 2.51(4) μ_B and 2.56(5) μ_B for the ⟨100⟩ and ⟨001⟩ directions, respectively. They are close to the expected value for the free Ce^{3+} ion (2.54 μ_B). To estimate θ_P, it is important to exclude the contribution of the excited CEF states because the estimation of θ_P is affected by not only the magnetic interaction but also by the population of the excited CEF states. Because the most significant interaction for the ordered state is that with the CEF ground state, θ_P should be estimated from a sufficiently lower temperature range than the first excitation energy of the CEF. Therefore, θ_P is obtained from CW fitting in the temperature range 4 K and 20 K, because the first excitation energy of the CEF is estimated at approximately 170 K as described in the result of the specific heat measurements. The obtained $\theta_P = -6.2$ K suggests an effective antiferromagnetic interaction between the $4f$ electrons in the lowest CEF states.

In frustrated magnets, the strength of the frustration is often measured by $|\theta_P|/T_N$. For Ce_2Pt_2Pb, $|\theta_P|/T_N$ is estimated as 1.8, which is obviously smaller than that of other typical frustrated magnets with transition elements [17–19]. However, the ytterbium analog Yb_2Pt_2Pb also shows a small $|\theta_P|/T_N$ (∼2.4) although it exhibits explicitly frustrated behaviors such as successive anomaly under the magnetic fields [14,20,21]. Therefore, a small $|\theta_P|/T_N$ may not imply a small frustration in $4f$ magnets. Besides, it is noteworthy that the CW law well reproduces the paramagnetic susceptibility below approximately 50 K as shown in the main panel of Fig. 2. This result implies that the mean-field approximation is sufficient to reproduce the magnetic behavior above T_N in Ce_2Pt_2Pb. In contrast with this behavior, the susceptibility of Yb_2Pt_2Pb shows a broad maximum slightly above T_N, which is interpreted as a manifestation of the short-range correlation due to the influence of the frustration [14]. Therefore, we have found no evidence indicating the influence of the frustration from the susceptibility in Ce_2Pt_2Pb.

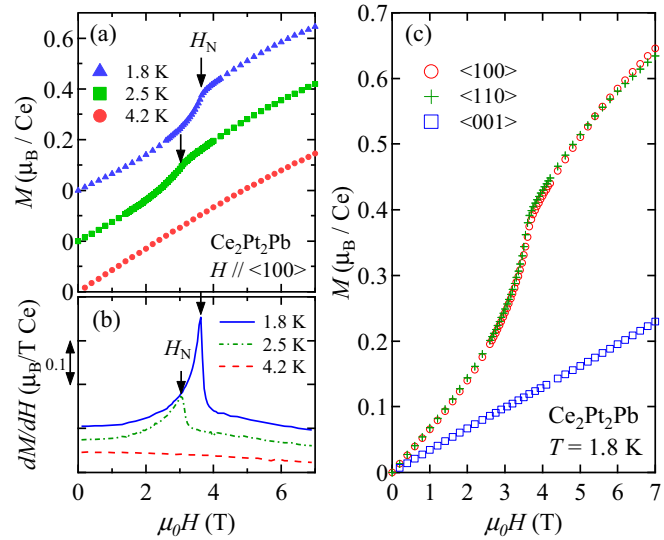

FIG. 3. (a) Magnetization curves at fixed temperatures, 1.8, 2.5, and 4.2 K. The magnetic field is applied along the ⟨100⟩ direction. (b) Field dependence of differential susceptibilities obtained from the data of panel (a). Each plot is vertically shifted for clarity. Solid arrows in panels (a) and (b) represent the phase transition field H_N. (c) Magnetic field dependence of magnetizations at 1.8 K along the ⟨100⟩, ⟨110⟩, and ⟨001⟩ directions.

C. Magnetization

Figure 3(a) shows the magnetization curves along the ⟨100⟩ direction at several fixed temperatures. An abrupt increase in the magnetization appears around the field H_N on both the 2.5 K and 1.8 K curves. This increase is observed as a sharp peak anomaly on the field derivative of magnetization dM/dH as shown in Fig. 3(b). The anomaly at H_N becomes steep and shifts to a slightly higher field with decreasing temperature. While the temperature is held above T_N, no anomaly appears on the magnetization curve as shown by the curve at 4.2 K.

Figure 3(c) shows isothermal magnetization curves at 1.8 K ($< T_N$) along three symmetrical directions of the tetragonal symmetry: ⟨100⟩, ⟨110⟩, and ⟨001⟩. The magnetization curves along the ⟨100⟩ and ⟨110⟩ directions show no significant difference under 7 T. This is not a symmetrical result of tetragonal crystals. Because the local symmetry of the Ce^{3+} site is orthorhombic C_{2v}, the magnetizations along the ⟨100⟩ and ⟨110⟩ directions are generally different from each other. These magnetizations become identical when the CEF ground state of the Ce^{3+} ion has an isotropic magnetic moment in the (100) plane. The magnetization curve along ⟨001⟩ retains a lower magnetization than those along the other two directions. It shows only a linear increase without any significant anomalies below 7 T. The anisotropic magnetization curves indicate that the CEF ground state has an easy plane type anisotropy in the (100) plane. That is, the (001) plane and the ⟨001⟩ direction correspond to magnetically easy plane and hard direction, respectively. Furthermore, the antiferromagnetic ordered state

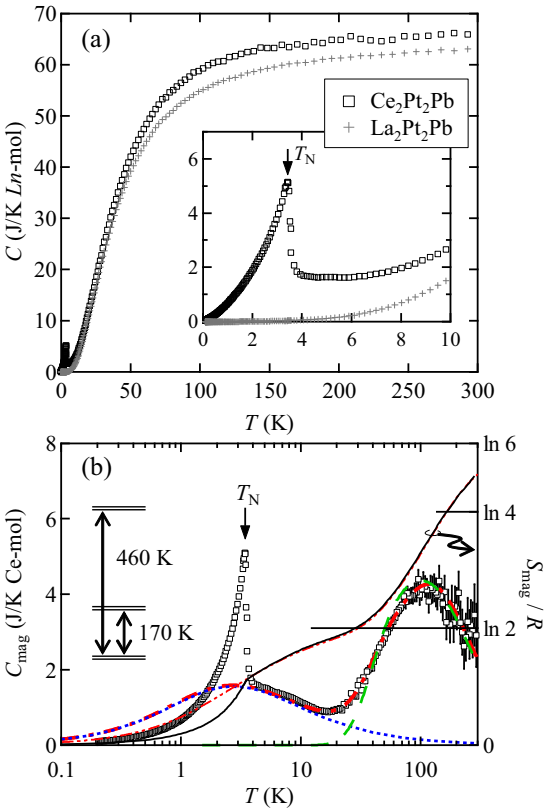

FIG. 4. (a) Temperature dependences of the specific heat of Ce_2Pt_2Pb and La_2Pt_2Pb under a zero magnetic field. Inset shows a magnified scale below 10 K. The solid arrow indicates the phase transition temperature T_N. (b) Temperature dependences of the magnetic specific heat of Ce_2Pt_2Pb. Vertical lines from square markers indicate the error bar. The dotted, broken, and single-dotted broken lines represent the calculated specific heats for the spin-1/2 Kondo model [22], the Schottky model for CEF, and a model including both the above effects [23]. The energy scheme of the CEF is denoted in the left side of the panel. Solid and double-dotted broken lines show the temperature dependences of the magnetic entropy associated with the experiment and the calculation for the single-dotted broken line, respectively. The horizontal lines are eye guides.

seems to have a rotational symmetry because no significant difference is observed within the (001) plane below H_N.

D. Specific heat

Figure 4(a) shows the specific heat of Ce_2Pt_2Pb and its nonmagnetic analog La_2Pt_2Pb. The specific heat of Ce_2Pt_2Pb is larger than that of La_2Pt_2Pb over the entire measured range. The inset shows a magnified scale for the low temperature range. The large difference between the specific heats of Ce_2Pt_2Pb and La_2Pt_2Pb means that the magnetic contribution of the specific heat become dominant with decreasing temperature. A pronounced peak at $T_N = 3.4$ K is a clear manifestation of a phase transition. The specific heat also implies that the small broad peak reported in Ref. [16] is attributed to a broadening of this phase transition. This broadening often arises from some types of disturbance factors lurking in the polycrystalline sample, for instance, lattice distortion, inhomogeneity, or vacancy of the elements. In fact, our *preliminary* synthesized samples had distributed transition temperatures ($T_N = 2.7 \sim 3.4$ K) although they were single crystals. This probably resulted from the distribution of the composition rate of the elements due to a synthesizing procedure. Therefore, the ordered phase of this compound may be sensitive to the disturbance factors. In this paper, we have used carefully synthesized samples to reveal the inherent properties of Ce_2Pt_2Pb. Our current samples exhibit the phase transition at $T_N = 3.4 \pm 0.1$ K.

Assuming that the nonmagnetic contributions of Ce_2Pt_2Pb are the same as the specific heat of La_2Pt_2Pb, the magnetic specific heat C_{mag} of Ce_2Pt_2Pb is obtained by subtracting the specific heat of La_2Pt_2Pb from that of Ce_2Pt_2Pb. The obtained C_{mag} is shown in Fig. 4(b). A broad hump is found at approximately 100 K, which is interpreted as the contribution from the thermal excitation of the split $J = 5/2$ multiplet of the Ce^{3+} ion under the CEF. The calculated specific heat of the Ce^{3+} ions under C_{2v} local symmetry is shown as a broken line in Fig. 4(b), which reasonably represents the experimental result around the hump. The excitation energies of the first and second excited states are estimated as 170 K and 460 K from the ground state, respectively.

The solid curve in Fig. 4(b) represents the magnetic entropy $S_{mag}(T)$ indexed on the right axis. Note that we estimate the entropy at the lowest measured temperature (0.2 K) as $S_{mag}(0.2\,\mathrm{K}) = 0.088$ J/K Ce-mol assuming T-linear dependence of C_{mag}/T below the temperature as described in the last paragraph of this subsection. The entropy reaches $R \ln 2$ at approximately 30 K, which indicates that the magnetic order arises from the ground state degeneracy of the CEF, a Kramers doublet. At T_N, S_{mag} reaches 0.55 $R \ln 2$ per cerium mole. Consequently, the remaining entropy of the Kramers doublet is released above T_N. Because Ce_2Pt_2Pb has metallic conductivity as shown later, the Kondo effect should be examined as the origin of the small entropy at T_N before discussing the magnetic frustration. We find that a spin-1/2 Kondo model (resonance level model [22]),

$$C = \frac{N_A \Delta}{\pi T}\left(1 - \frac{\Delta}{2\pi k_B T}\psi'\left(\frac{1}{2} + \frac{\Delta}{2\pi k_B T}\right)\right) \qquad (1)$$

with $\Delta/k_B = 5.5$ K reasonably represents C_{mag} between 4 K and 20 K, where N_A, k_B, and ψ' are the Avogadro constant, Boltzmann constant, and the derivative of the digamma function, respectively. This result indicates that the Kondo effect notably affects this compound and the Kondo temperature $T_K \sim \Delta/k_B$ has the same order of magnitude as T_N.

The hybridization between the conduction electrons and the *excited* CEF doublets slightly modifies the specific heat from their simple sum. The calculated specific heat using a model including the modification [23] shows excellent agreement with the measured specific heat above 4 K, where the model requires only one additional parameter $\Gamma_1 = 25$ K representing the half width at half maximum of the spectral density for the first excited doublet of the CEF. The calculated entropy shows good agreement with our experimental result over the temperature range. Although these agreements violate due to the magnetic order below T_N, these Kondo models also give a paramagnetic T-linear coefficient of the specific heat $\gamma_p \sim 1.55$ J/K Ce-mol that assumes no magnetic order at absolute zero temperature. Large γ_p means strong hybridization of

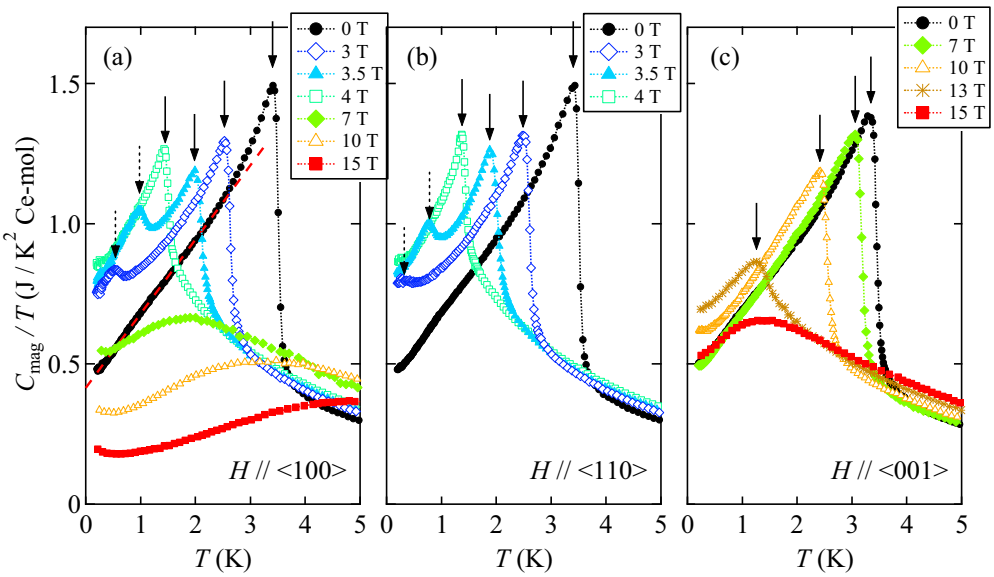

FIG. 5. Temperature dependences of the magnetic specific heat divided by the temperature C_{mag}/T of Ce_2Pt_2Pb. Solid and broken arrows indicate the phase transition temperatures. The directions of the applied field are along ⟨100⟩, ⟨110⟩, and ⟨001⟩ for panels (a), (b), and (c), respectively. The broken line in panel (a) represents the result of the linear fit.

conduction and f electrons in the paramagnetic phase, but it is partially suppressed for less than one third of the value by the antiferromagnetic order in Ce_2Pt_2Pb.

Figure 5 shows the magnetic contribution to the specific heat divided by the temperature, C_{mag}/T, under several magnetic fields. Applying the magnetic field shifts the peak at T_N to the lower temperature side regardless of the field direction. When the field is applied along the ⟨100⟩ or ⟨110⟩ directions, two successive peaks appear under 3 and 3.5 T as shown in Figs. 5(a) or 5(b). These features suggest the emergence of two successive phase transitions within the field. Further increasing the field suppresses the peak to zero temperature at approximately 6 T. Above this field, a broad hump appears and shifts to the high temperature side as the field increases, as shown in Fig. 5(a). This behavior may not correspond to a phase transition but may originate from the Zeeman splitting of the magnetic moment in the paramagnetic phase. The slight upturns observed in low-temperature and high-field conditions, for example below 0.5 K under 15 T, can probably be attributed to the nuclear contribution. Besides, when the field is applied along the ⟨001⟩ direction, T_N retains finite temperatures until 13 T as shown in Fig. 5(c). No successive transition is observed for this direction.

From a comparison between Figs. 5(a) and 5(b), one can notice that the specific heat behaves in the same manner regardless of the applied directions of the field. This result sharply contrasts with that of Yb_2Pt_2Pb. The specific heat of Yb_2Pt_2Pb varies by applied field direction even in the ⟨100⟩ and ⟨110⟩ directions, whose origin is the strong easy-axis-type anisotropy of the Yb moments. On the other hand, in Ce_2Pt_2Pb, similar results for the ⟨100⟩ and ⟨110⟩ directions of the field strongly suggest that the ordered phase has an approximately continuous rotational symmetry within the (001) plane under a zero magnetic field. This result also implies a rather easy-plane type anisotropy that lies on the (001) plane for each Ce moment.

From the specific heat measurement, we can estimate the Sommerfeld coefficient γ which reflects the density of states of itinerant electrons at the Fermi level. We estimate $\gamma = 414\,\mathrm{mJ/K^2}$ Ce-mol from a curve fitting using the formula $C_{mag}(T)/T = \gamma + \beta' T$ below 2.5 K. Because the temperature range is below T_N, the coefficient of the second term $\beta' = 0.265\,\mathrm{J/K^2}$ Ce-mol may be interpreted as a two-dimensional system with k-linear dispersion bosons, e.g., two-dimensional antiferromagnetic magnons.

E. Electrical resistivity

Figure 6 shows temperature dependences of the electrical resistivity on the directions of current flow ⟨100⟩ ($\rho_{\langle 100\rangle}$) and ⟨001⟩ ($\rho_{\langle 001\rangle}$). The absolute value of the resistivity depends on the direction of current flow, which probably implies an anisotropic shape of the Fermi surface. At the ordering temperature T_N, $\rho_{\langle 100\rangle}$ and $\rho_{\langle 001\rangle}$ show a kink anomaly and a step anomaly, respectively. These anomalies could be interpreted as the combined effect of reduction in the spin disorder scattering and the superzone gap opening below T_N. However, an estimation of the superzone gap by the formula [24] results in a negative coefficient for the gap term. This result may reflect the fact that the Kondo temperature has the same order as the antiferromagnetic ordering temperature.

Our samples show a somewhat large residual resistivity (RR), although they exhibit clear anomalies at the phase transition temperature. The RR of our sample is $\rho_0 = 58$ (64) $\mu\Omega$ cm along the ⟨100⟩ (⟨001⟩) axis. This is a rather large RR for metallic compounds, which may imply that disturbances still remain in our sample. The disturbances possibly originate from a small amount of impurity that cannot be detected by XRD, or strain distortion due to the thermal strain of the crucible. Other isostructural Ce-based compounds typically have the same order as the RR [10,16,25–27], while a single crystalline sample of Ce_2Ge_2Mg shows a somewhat lower RR

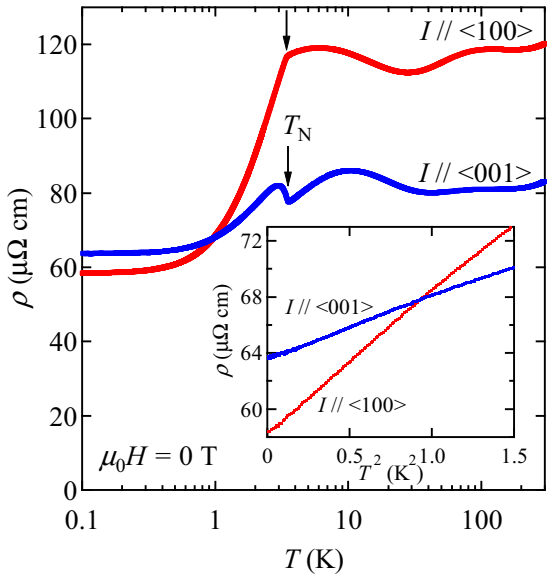

FIG. 6. Temperature dependences of the electrical resistivity with the current flowing along the ⟨100⟩ and ⟨001⟩ directions. The solid arrows represent the transition temperature T_N. The inset shows the squared-temperature dependence of the resistivity below approximately 1.2 K.

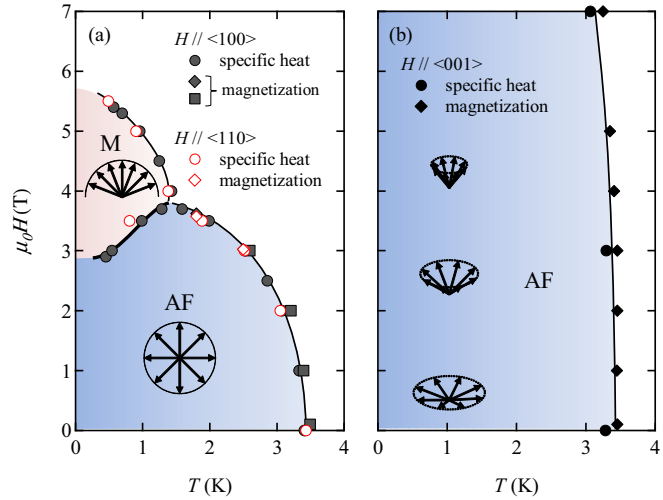

FIG. 7. Temperature-field phase diagrams of Ce_2Pt_2Pb. Circle markers indicate the phase transition temperature obtained from C_{mag}/T. Diamond and square markers indicate phase transition points obtained from the temperature and the field dependences of the magnetization, respectively. Panels (a) and (b) represent the phase diagrams for the field along the ⟨100⟩ and ⟨001⟩ directions, respectively. Phase transition points under the field along the ⟨110⟩ direction are superposed in the panel (a). AF and M represent the ordered phases of the lower- and higher-field sides, respectively. The magnetic structures are depicted by the arrows with a dotted circle, where the arrows and the circles represent the magnetic moments and the (001) plane, respectively.

(∼7.6) $\mu\Omega$cm. They have a residual resistivity rate (RRR) that is less than 10. On the other hand, single crystalline Yb_2Pt_2Pb has a rather small RR ∼1 $\mu\Omega$ cm and a large RRR ∼20 [16,21]. Because high-quality Ce_2Ge_2Mg and Yb_2Pt_2Pb samples are prepared with a self-flux method, crystal growing methods are considered to dominantly determine the transport properties of these compounds. In comparison with the self flux method, our Bridgman method may lack the purification processes that remove impurities from the crystal. However, the clear phase transition observed in the present Ce_2Pt_2Pb samples implies that the origins of large RR do not strongly disturb the magnetic order. Further purification of the sample is a future work.

At a higher temperature than T_N, both $\rho_{\langle 100\rangle}$ and $\rho_{\langle 001\rangle}$ exhibit two broad humps at approximately 10 K and 100 K. These humps could be interpreted as the dense Kondo effect with the CEF [28]. Looking from the higher-temperature side, the hump around 100 K is attributed to the scattering effect due to CEF excitations, while that of 10 K is a manifestation of the formation of the coherent Kondo lattice by f electrons; therefore, the resistivity is suppressed with decreasing temperature below approximately 10 K. As a result, the f electrons in Ce_2Pt_2Pb should construct the heavy-fermion state sufficiently below 10 K, which is consistent with the squared-temperature dependence of the resistivity below approximately 1 K as shown in the inset of Fig. 6. From curve fitting with the formula $\rho(T) = \rho_0 + AT^2$ to the resistivity lower than 1.0 K, we obtain the coefficients A as 10.3 and 4.60 $\mu\Omega\,\mathrm{cm/K^2}$ for $\rho_{\langle 100\rangle}$ and $\rho_{\langle 001\rangle}$, respectively. These large values of A are often observed in typical heavy-fermion compounds.

IV. DISCUSSION

Figure 7 shows the T-H phase diagrams of Ce_2Pt_2Pb obtained from the present work. The phase transition line represented by the thin solid line corresponds to the phase transition temperature T_N and field H_N. This line divides the ordered phases from the paramagnetic (or field induced ferromagnetic) phase. The phase diagrams depend on the direction of the field reflecting the magnetic anisotropy of this compound. When the field is applied along the ⟨100⟩ direction, as shown in Fig. 7(a), the transition temperature T_N decreases with increasing field and changes in slope at approximately 3.8 T; then it finally collapses to zero temperature between 5.5 and 6 T. The ordered phases below T_N are separated into two phases by another phase transition line represented by a thick solid line that corresponds to the lower-temperature transition among the successive phase transitions observed in the specific heat. Applying the field along the ⟨110⟩ direction almost reproduces the phase diagram along the ⟨100⟩ direction of the field. Besides, when the field is applied along the ⟨001⟩ direction, the AF phase is monotonically suppressed by the field.

Then, we discuss possible magnetic structures of Ce_2Pt_2Pb on the basis of our macroscopic results. As shown in Fig. 7(a), the ⟨100⟩ and ⟨110⟩ directions of the fields yield almost identical magnetic phase diagrams. This feature implies the possibility of rotational symmetry in the (001) plane for the AF phase. The magnetization and the specific heat show only a negligibly small difference between these directions. These results could be interpreted by a helical-type antiferromagnetic structure in the AF phase [29–31], which is predicted in the Shastry-Sutherland Heisenberg model [32,33]. This scenario is consistent with the fact that the M phase only emerges under

the field along the (001) plane (⟨100⟩ and ⟨110⟩ directions) because the helical-fan transition emerges under the field along the helical plane [29]. The emergence of the M phase also provides information on the origin of the helical structure. Helical structures are able to stabilize under frustrated interactions or antisymmetric exchange (Dzyaloshinskii-Moriya, DM) interaction; however, their transitions show different magnetization curves [34,35]. The helical structures stabilized by the frustrated interactions change into fan structures under the field along the helical plane, whereas the helical structures stabilized by DM interaction show no fanlike phase under the field. In the later case, the AF phase directly changes into the paramagnetic phase because the sign of the interaction energy is linked to the sign of the angle between the magnetic moments. The emergence of the M phase indicates that the possible helical structure in the AF phase is unlikely to originate from the DM interaction in Ce_2Pt_2Pb. The possible frustrated interactions probably originate from the RKKY interaction whose sign depends on the distance between the magnetic moments. Besides, the large Sommerfeld coefficient and superzone-gap-like behavior imply that the helical structure is possibly due to itinerant f electrons [36,37]. We conclude this paragraph with the remark that microscopic measurements such as neutron diffraction measurement are necessary to confirm the magnetic structure of Ce_2Pt_2Pb, although macroscopic results are reasonably explained by the helical scenario.

Finally, let us examine aspects of the heavy-fermion behavior and of the geometrical frustration effect in Ce_2Pt_2Pb. The large γ value (414 mJ/K^2Ce-mol) of the specific heat and obvious T^2 dependence accompanying the humplike behavior of the resistivity imply significant hybridization between the conduction band and the f electrons (c-f hybridization) in this compound. From these values, we obtain the ratio A/γ^2 as 6.0×10^{-5} and 2.7×10^{-5} $\mu\Omega/\mathrm{cm(mJ/K^2Ce\text{-}mol)^{-2}}$ from the resistivities along the ⟨100⟩ and ⟨001⟩ directions, respectively. These ratios are on the same order as the Kadowaki-Woods relation $A/\gamma^2 \simeq 1 \times 10^{-5}$ $\mu\Omega/\mathrm{cm(mJ/K^2Ce\text{-}mol)^{-2}}$, although they are somewhat larger than the relation. The c-f hybridization yields the RKKY interaction and the Kondo effect, which may explain the heavy fermion in Ce_2Pt_2Pb. The rather small released entropy at T_N, about 55% of R ln2, is also attributed to the itinerant nature of the f electrons resulting from the Kondo effect. This scenario is confirmed by the good agreement between the measured and calculated specific heats with $T_K \sim 5.5$ K. Therefore, the physical properties of Ce_2Pt_2Pb can be explained by the RKKY interaction and the Kondo effect yielded by the c-f hybridization.

On the other hand, evidence of the influence of the geometrical frustration is hardly found from the present results. The obtained strength of frustration from Ce_2Pt_2Pb ($|\theta_P/T_N| \sim 1.8$) is rather small and may not be a relevant index of the frustration in an f-electron compound. The magnetic susceptibility obeys the CW law even around T_N, which means there is no significant contribution of the short-range order around T_N. Contrary to this, in other frustrated compounds [17,19] and Yb_2Pt_2Pb [14], a susceptibility maximum that manifests as the development of the short-range order is clearly observed slightly above T_N. In addition, the small released entropy at T_N should be attributed to the Kondo effect as mentioned above. From these results, we hardly see any evidence supporting the influence of the geometrical frustration in Ce_2Pt_2Pb.

V. CONCLUSION

We have successfully grown single crystalline samples of Ce_2Pt_2Pb and measured their powder XRD, specific heat, magnetization, and electrical resistivity. An antiferromagnetic phase transition is found around 3.4(1) K under a zero magnetic field. The magnetic anisotropy of this compound is found to be the easy-plane type. The T-H phase diagrams under the field along three symmetrical directions of the crystallography, ⟨100⟩, ⟨110⟩, and ⟨001⟩, can be explained by the helical and the fan structures. The γ value, squared-temperature dependence of the resistivity, and their reasonable agreement with the Kadowaki-Woods relation suggest construction of the heavy-fermion state in Ce_2Pt_2Pb. The small entropy released at T_N is also explained by the itinerant nature of f electrons. We conclude that the ground state of Ce_2Pt_2Pb is not the frustration-driven QCP as previously reported, but an antiferromagnet with heavy-fermion properties.

[1] L. Balents, Nature (London) **464**, 199 (2010).
[2] P. Coleman and A. H. Nevidomskyy, J. Low Temp. Phys. **161**, 182 (2010).
[3] Q. Si, Phys. Status Solidi B **247**, 476 (2010).
[4] B. H. Bernhard, B. Coqblin, and C. Lacroix, Phys. Rev. B **83**, 214427 (2011).
[5] J. H. Pixley, R. Yu, and Q. Si, Phys. Rev. Lett. **113**, 176402 (2014).
[6] L. Su and P. Sengupta, Phys. Rev. B **92**, 165431 (2015).
[7] R. Pöttgen, A. Fugmann, R.-D. Hoffman, U. Rodewald, and D. Niepmann, Z. Naturforsch. **55b**, 155 (2000).
[8] G. Melnyk, L. D. Gulay, and W. Tremel, J. Alloys Compd. **528**, 70 (2012).
[9] B. S. Shastry and B. Sutherland, Physica B **108**, 1069 (1981).
[10] D. Kaczorowski, P. Rogl, and K. Hiebl, Phys. Rev. B **54**, 9891 (1996).
[11] S. Rayaprol and R. Pöttgen, Phys. Rev. B **72**, 214435 (2005).
[12] J. G. Sereni, M. Gómez-Berisso, A. Braghta, G. Schmerber, and J. P. Kappler, Phys. Rev. B **80**, 024428 (2009).
[13] S. Mock, A. Faisst, and H. v. Löhneysen, Phys. Rev. B **56**, 335 (1997).
[14] A. Ochiai, S. Matsuda, Y. Ikeda, Y. Shimizu, S. Toyoshima, H. Aoki, and K. Katoh, J. Phys. Soc. Jpn. **80**, 123705 (2011).
[15] L. S. Wu, W. J. Gannon, I. A. Zaliznyak, A. M. Tsvelik, M. Brockmann, J.-S. Caux, M. S. Kim, Y. Qiu, J. R. D. Copley, G. Ehlers, A. Podlesnyak, and M. C. Aronson, Science **352**, 1206 (2016).
[16] M. S. Kim and M. C. Aronson, J. Phys.: Condens. Matter **23**, 164204 (2011).

[17] M. Niel, C. Cros, G. L. Flem, and P. Hagenmuller, Physica B **86-88**, 702 (1997).
[18] K. Takeda, K.Ubukoshi, T. Haseda, and K. Hirakawa, J. Phys. Soc. Jpn. **53**, 1480 (1984).
[19] H. Ueda, J.-I. Yamaura, H. Mitamura, T. Goto, H. A. Katori, H. Takagi, and Y. Ueda, J. Magn. Magn. Mater. **310**, 1275 (2007).
[20] Y. Shimura, T. Sakakibara, K. Iwakawa, K. Sugiyama, and Y. Ōnuki, J. Phys. Soc. Jpn. **81**, 103601 (2012).
[21] K. Iwakawa, Y. Hirose, K. Enoki, K. Sugiyama, T. Takeuchi, F. Honda, M. Hagiwara, K. Kindo, T. Nakano, Y. Nozue, R. Settai, and Y. Ōnuki, J. Phys. Soc. Jpn. **81**, SB058 (2012).
[22] K. D. Schotte and U. Schotte, Phys. Lett. A **55**, 38 (1975).
[23] M. A. Romero, A. A. Aligia, J. G. Sereni, and G. Nieva, J. Phys.: Condens. Matter **26**, 025602 (2014).
[24] N. H. Andersen, *Crystalline Electric Field and Structural Effects in f-Electron Systems*, edited by J. E. Crow, R. P. Guertin, and T. W. Mihalisin (Plenum Press, New York, 1980), p. 373.
[25] R. Hauser, H. Michor, E. Bauer, G. Hilscher, and D. Kaczorowski, Physica B **230-232**, 211 (1997).
[26] D. Kaczorowski and L. D. Gulay, J. Alloys Compd. **442**, 169 (2007).
[27] J. G. Sereni, M. Gómez Berisso, G. Schmerber, and J. P. Kappler, Phys. Rev. B **81**, 184429 (2010).
[28] S. Kashiba, S. Maekawa, S. Takahashi, and M. Tachiki, J. Phys. Soc. Jpn. **55**, 1341 (1986).
[29] T. Nagamiya, K. Nagata, and Y. Kitano, Prog. Theor. Phys. **27**, 1253 (1962).
[30] Y. Kitano and T. Nagamiya, Prog. Theor. Phys. **31**, 1 (1964).
[31] K. Inomata and T. Oguchi, J. Phys. Soc. Jpn. **25**, 1533 (1968).
[32] M. Albrecht and F. Mila, Europhys. Lett. **34**, 145 (1996).
[33] C. H. Chung, J. B. Marston, and S. Sachdev, Phys. Rev. B **64**, 134407 (2001).
[34] T. Moriya and T. Miyadai, Solid State Commun. **42**, 209 (1982).
[35] Y. Togawa, Y. Kousaka, K. Inoue, and J. Kishine, J. Phys. Soc. Jpn. **85**, 112001 (2016).
[36] M. Tachiki and T. Nagamiya, Phys. Lett. **3**, 214 (1963).
[37] K. Yamasaki, J. Phys. Soc. Jpn. **23**, 1209 (1967).